ELSEVIER

Biophysical Chemistry 78 (1999) 33–41

Biophysical Chemistry

Changes in water structure induced by a hydrophobic solute probed by simulation of the water hydrogen bond angle and radial distribution functions

Bhupinder Madan, Kim Sharp*

The Johnson Research Foundation, Department of Biochemistry and Biophysics, University of Pennsylvania, Philadelphia, PA 19104-6059, USA

Received 10 August 1998; received in revised form 2 November 1998; accepted 23 November 1998

Abstract

In order to better characterize changes in water structure induced by a hydrophobic solute the oxygen–oxygen and hydrogen–hydrogen radial distribution functions ($g_{oo}(r)$, $g_{hh}(r)$) and the hydrogen bond angle distribution function $p(\theta)$ for water molecules in the first hydration shell of the tetramethyl ammonium (TMA) cation were computed using Monte Carlo simulations. $g_{oo}(r)$ and $g_{hh}(r)$ were corrected for the effect of solute volume exclusion on the local solvent density so that intrinsic structural changes independent of local solvent density variations could be detected. Comparison of $g_{hh}(r)$ of TMA's first hydration shell water with $g_{hh}(r)$ for bulk water shows subtle but clear evidence of structure formation induced by the ion. These changes in $g_{hh}(r)$ are very similar to those seen experimentally for larger tetra-alkyl ammonium ions in previous neutron diffraction experiments. Larger changes in $p(\theta)$ in the first hydration shell of TMA were seen. Comparison of changes in $p(\theta)$ with changes in $g_{oo}(r)$ and $g_{hh}(r)$ show that the angle distribution function provides the most sensitive way to analyze water structure changes associated with hydrophobic solvation.

Keywords: Solvation; Hydration; Heat capacity; Hydrophobic effect

1. Introduction

Understanding the hydrophobic effect has been an important goal in physical chemistry and biophysics for many decades because of the dominant role it plays in many important phenomena in biology, such as protein folding, protein–protein interactions, protein–DNA interactions and micelle formation. The original suggestion of Frank and Evans that the structure of water changes to a more ordered state around hydrophobic groups on their exposure to water [1] has been widely accepted, and this is supported by the measured decrease in entropy upon hydra-

* Corresponding author. Tel.: +1 215 5733506; fax: +1 215 8984217; e-mail: sharp@crystal.med.upenn.edu

0301-4622/99/$ - see front matter
PII: S0301-4622(98)00227-0

tion of nonpolar compounds at room temperature [2]. However, many polar and ionic groups also induce ordering of water since they have negative entropies of hydration too [3–5]. The distinction is that polar hydration produces a decrease in heat capacity, whereas hydrophobic hydration produces an increase in heat capacity [2,3,6–9], indicating a qualitative difference in the water structuring.

In spite of the wide agreement about the general features of the hydrophobic effect, there are remarkably few direct experimental measurements that reveal the specific changes in water structure around apolar solutes in solution. One difficulty is that there are many alternative ways to characterize water structure, including radial and angular distribution functions, coordination number, H-bond lengths and angles, and formation of multimeric water assemblies, such as pentamers and clathrates [10], but few are experimentally accessible. Techniques, such as infrared, Raman, and magnetic resonance spectroscopy provide direct evidence of an increase in the 'strength' of hydrogen bonds, and a decrease in motion within the hydration shell of hydrophobic solutes [11,12], but these changes cannot be easily translated into specific structural changes and interpretation of results from these kind of experiments is model-dependent. X-ray scattering can provide a direct measure of changes in the water oxygen–oxygen correlation function, $g_{oo}(r)$ [13], but this proves to be a rather insensitive measure of structural changes, partly because the scattering contains signal from both hydration and bulk (unperturbed) water oxygens, and from radial distributions for every solute heavy atom-water oxygen. Another persistent difficulty is that it is hard to dissolve sufficient nonpolar molecules in water due to the very nature of the hydrophobic effect, and therefore to produce enough perturbation to be seen in experimental studies. Thus the bulk of the work on structure of water in solutions has been done on polar and ionic compounds.

To date the most sensitive and direct measure of water structure changes is neutron scattering using isotope substitution. This allows individual radial distribution functions to be extracted. In particular it allows for direct determination of hydrogen–hydrogen radial distribution function $g_{hh}(r)$ and, more indirectly, orientational correlation functions [14–16]. These functions are expected to be particularly informative about structural changes in hydrating waters since there is a high degree of orientational or angular ordering in liquid water. One might conceive, for example, of changes in hydrogen bond angle that could result in significant changes in the water $g_{hh}(r)$, but which lie within very similar $g_{oo}(r)$ envelopes, and thus be largely invisible to techniques that measure O–O distances, like X-ray scattering or H-bond length/strength, like IR spectroscopy.

In a series of elegant experimental studies using the hydrophobic tetra-alkyl ammonium (TAA) cations Turner et al. have solved the insolubility/signal sensitivity problem [14–16]. These ions are soluble in water but show increasingly hydrophobic behavior (positive hydration heat capacities) as the size of alkyl groups is increased. Using neutron scattering, Turner et al. saw sharpening in $g_{hh}(r)$ around the larger TAA cations, indicating increased structure, but the effects are not large [16]. For the smallest TAA ion, tetramethyl ammonium (TMA), no significant change in $g_{hh}(r)$ was seen [14], yet this ion is 'hydrophobic' as defined by a negative hydration entropy and a positive hydration heat capacity [4,17].

Due in part to lack of direct experimental measures of water structure changes, there have been extensive computer simulations of hydrophobic hydration. The conclusions about water structuring drawn from these studies are not clear-cut either. For example from analysis of radial distribution functions Tobias and Brooks found little ordering of water around butane [18] and Wallqvist found little perturbation of water structure in the vicinity of methane [19]. On the other hand, by comparing solute-water oxygen and solute-water hydrogen radial distribution functions, Pangali et al. concluded that waters tend to be oriented with hydrogen bonds parallel to apolar solute surfaces [20]. While many simulation studies have focused primarily on radial distribution functions, the importance of analysing the angular component of water structure has been recognized [21]. Direct analysis of the water

dipolar and hydrogen bond direction vectors at solute surfaces shows that waters tend to be oriented with hydrogen bonds parallel to apolar solute surfaces [22]. However, a different orientation of water is seen at flat hydrophobic surfaces [23] and solute surface regions with different curvatures [24]. At the same time, computer simulations produce quite reasonable thermodynamics of solvation [25–28]. This suggests that sufficient water structuring to account for the observed entropy decreases is occurring in these simulations, but is difficult to say what structural changes are primarily responsible, in part because there are alternative ways to characterize water structure.

This study has two goals: first, to simulate the structure of water around the hydrophobic cation TMA, and compare $g_{hh}(r)$ in the first hydration shell to that determined experimentally [14,16]. Second, to compare different measures of water structuring. In particular, we would like to reconcile the apparently small structural changes seen in some experiments and theoretical simulations with the significant ordering implied by the unfavorable entropy of hydration. We base our structural analysis on the random network model (RNM) of water [29,30]. In this model three water structure parameters are considered: the mean and standard deviation in water–water H-bond length, r and s, respectively, and the root mean square water–water H-bond angle, $\langle \theta^2 \rangle^{1/2}$. We have previously analyzed the structure of water around a variety of polar and hydrophobic solutes using this model, and have shown that it can provide a quantitative explanation of observed hydration heat capacities [31–33]. In this analysis, changes in $\langle \theta^2 \rangle^{1/2}$ were found to be the most important structural perturbation. Of particular relevance for the present study, RNM reproduces the observed differences in the sign of heat capacity of hydration for the cations K^+ and Cs^+ (negative) and TMA (positive). The latter is an indication that TMA acts as a hydrophobic group. Since the RNM analysis can account for the increase in heat capacity that characterizes hydrophobic solvation, it provides strong evidence that a structural analysis of hydrating waters based on this model focuses on the relevant structural changes.

2. Methods

A dilute solution of TMA was simulated by inserting one molecule of the solute into a box of 750 molecules of TIP4P water [34]. The OPLS potential function is used for the interaction between water and solute molecule [35]. This, in conjunction with the TIP4P water potential, provides accurate hydration free energies for a wide range of solutes. The configurations of the aqueous solutions of TMA were sampled using a Metropolis Monte-Carlo algorithm implemented in the program BOSS [36]. Periodic boundary conditions were used with a cutoff of 12.0 Å. The simulations were performed at 25°C and 1 atm. pressure. Flexibility of the solute molecules was not included. The systems were first equilibrated for 5×10^7 Monte Carlo steps, following which data was collected for 10 consecutive runs of 1×10^7 steps each.

From an initial simulation the first hydration shell of the solute was determined from the first minimum of the solute/water oxygen radial distribution function. During the data collection runs, an instantaneous configuration of the dilute solution was analyzed every 1000 steps. The values of the various interaction energies and radial distribution functions were computed from these configurations. For each configuration, water molecules were then classified as belonging to either the first hydration shell or the bulk water. The distance between all pairs of first shell water hydrogen atoms was computed and a distance frequency histogram accumulated throughout the whole run. A similar histogram was accumulated for the first shell oxygen–oxygen distance. A frequency histogram was collected for H-bond angles between two first shell waters (for waters within the H-bond cutoff distance of 3.4 Å. The H-bond angle, θ is defined as the angle between the O–H vector and the O–O vector, so a linear H-bond has an angle of zero. For a given water pair there are four possible O–H vectors—the one which makes the smallest angle is chosen. (See Madan and Sharp [31]).

The first shell hydrogen–hydrogen and oxygen–oxygen radial distribution functions were obtained from the distance frequency histograms and corrected for local solvent density variations as follows. The radial distribution function for solvent atom types X and Y, $g_{xy}(r)$, is obtained from the frequency histogram using:

$$g_{xy}(r) = n_{xy}(r)/\left(V(r)\rho_y\right) = \rho_{xy}(r)/\rho_y \qquad (1)$$

where $n_{xy}(r)$ is the frequency of finding an atom of type Y between r and $r+\delta r$ of an atom of type X, ρ_y is the bulk density of atom type Y, and $\rho_{xy}(r)$ is the average local density of Y at a distance r from X. In a homogeneous solvent, we simply have $V(r) = 4\pi r^2\delta r$, the volume of a spherical annulus of radius r, thickness δr centered on X. However, when considering the radial distribution function within a solute's first hydration layer, for a given r only part of the annulus may lie within the hydration shell depending on the solute radius, r_s, the hydration shell thickness, t, and the position of the atom X, r_x (Fig. 1). The annulus thus crosses three regions: the hydration shell, the bulk solvent, and the solute volume. Only waters within the first region can contribute to the first shell radial distribution functions. Thus both solute exclusion and bulk exclusion result in a lower local density. This effect is independent of any intrinsic change due to solvent structural changes and must be corrected for before changes in radial distribution function reflecting these solvent structure changes can be extracted from the simulations. Turner et al. corrected their experimental radial distribution functions for solute volume exclusion assuming a spherical cavity using a Fourier transform approach [16]. In this study we used two alternative approaches, an analytical approximation and a Monte-Carlo technique, since these can easily be extended to account for the hydration shell effect too, and in the case of the Monte-Carlo method, to non-spherical solute geometries.

The solute cavity radius and hydration shell thickness, r_s and t, respectively, are obtained from the preliminary simulation used to determine the solute-water X (X = H or O) radial distribution. r_s and t are taken as the inner boundary and width of the first peak in this radial distribution function, respectively. A second data collection simulation is then run. In the analytical correction method, during accumulation of the distance frequency histogram the volume of the spherical annulus around each solvent atom X lying within the hydration shell, V_i, is computed as a function of r using r_s, t and that atom's current value of r_x using standard geometric formulae:

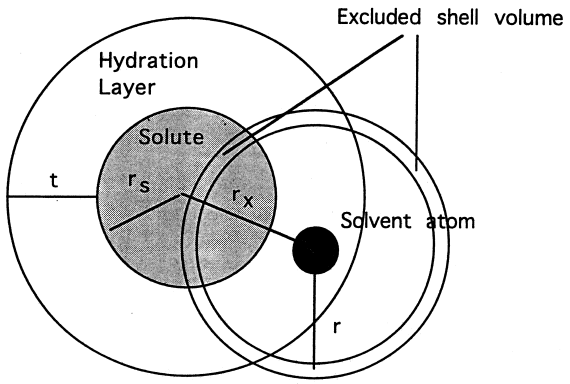

Fig. 1. Correction for variation in local solvent atom density due to solute volume and hydration shell exclusion.

$$V_i = 4\pi r^2\delta r - V_s - V_b \qquad (2)$$

where

$$\begin{aligned} V_s &= 2\pi r\delta r\left(r - (r^2 - r_s^2 + r_x^2)/2r_x\right) \\ &\qquad \text{for } |r_s - r| < r_x < (r_s + r) \\ &= 0 \qquad \text{for } r_x > (r_s + r) \text{ or } r_x \\ &\qquad < |r_s - r| \text{ and } r > r_s \end{aligned} \qquad (3)$$

and

$$\begin{aligned} V_b &= 2\pi r\delta r\left(r + (r^2 - r_b^2 + r_x^2)/2r_x\right) \\ &\qquad \text{for } |r_b - r| < r_x < (r_b + r) \\ &= 4\pi r^2\delta r \qquad \text{for } r_x < |r_b - r| \text{ and } r > r_b \\ &= 0 \qquad \text{for } r_x < |r_b - r| \text{and } r < r_b \end{aligned} \qquad (4)$$

where $r_b = r_s + t$. These annuli volumes are binned as a function of r and at the end of the simula-

tion are used to compute the average annulus volume lying within the hydration shell for each given r, $\langle V(r)\rangle$. $\langle V(r)\rangle$ is then used in Eq. (1) to obtain the radial distribution function from the distance frequency histograms.

In the Monte-Carlo method, points are randomly placed in a cubic volume large enough to enclose the solute and the hydration shell. The distance of each point from the solute center (r_x) is computed, and then each point is classified as lying within the solute ($r_x < r_s$), within the first solvation shell ($r_s < r_x < r_s + t$), or within bulk solvent ($r_s > r_s + t$). The radial distribution function for pairs of points lying within the first hydration shell, $g_{ran}(r)$ is computed using Eq. (1) with $V(r) = 4\pi r^2\delta r$. In effect $g_{ran}(r)$ is the radial distribution function expected for a structureless solvent accounting for solute volume and hydration shell exclusion. The uncorrected solvent radial distribution function from the solute simulation is also calculated using $V(r) = 4\pi r^2\delta r$ and then corrected by dividing through by $g_{ran}(r)$. Random configurations are generated until the distribution function converges. Using 1000 random configurations of 750 solvent points provided a well converged distribution, and took about 500s on a Silicon Graphics R10 000 processor.

3. Results

The hydrogen–hydrogen radial distribution function for the first hydration shell water molecules and for pure water are shown in Fig. 2. The peak corresponding to hydrogen–hydrogen distances for both the hydrogen atoms lying on the same water molecule (the intramolecular peak) is not shown in this figure because we use a rigid model of water, TIP4P, in our Monte Carlo simulations. Thus the first and second peaks in Fig. 2 should be compared to the second and third peaks, respectively in the corresponding radial distribution functions from neutron diffraction data. For the TMA hydration shell water results are shown for both the analytically corrected and Monte-Carlo corrected distributions, using the values $r_s = 4.5$ Å and $t = 6.4$ Å determined from the simulation. The two curves are indistinguishable and go to the expected limit of 1

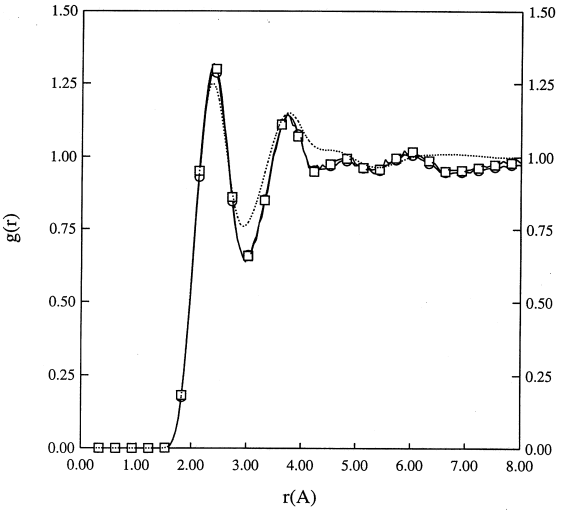

Fig. 2. The water hydrogen–hydrogen radial distribution function for pure water (···), for the first shell of TMA^+ using the analytical correction (○) or the Monte Carlo correction (□). The intramolecular peak has been suppressed on this plot.

at large distances, providing confirmation that the solute volume and hydration shell exclusion corrections are being applied correctly. The slight oscillations at large r probably result from sampling error, since the number of solvent pairs that lie within the hydration shell at larger distances is very small.

Relative to pure water the first peak of the radial distribution function for the hydrogen atoms in the hydration shell of TMA is higher than the corresponding function for pure water, while the first trough is deeper. The peak to well ratio for the two peaks are: 1.64 for pure water, 1.73 for the distribution function computed using an analytical correction for the solute volume/hydration shell exclusion, and 1.79 for the distribution function computed using a Monte Carlo correction. This sharpening is an indication of structure formation among water molecules in the hydration shell of TMA. This is clear evidence for the hydrophobic behavior of the TMA ion. This behavior for an ion, however, is not surprising in spite of the fact that ions normally do not show hydrophobic behavior. Experimental data show that TMA has a large and positive heat capacity of hydration of 36 cal/mol/K compared,

for example, to the value of −17 cal/mol/K for K^+ [4]. We previously computed the RNM parameters for the hydrogen bonds formed between water molecules in the hydration shell of the TMA ion [33]. We observed that the mean H-bond length decreased from 2.95 Å in pure water to 2.92 Å around TMA, while the RMS H-bond angle decreased from 29.4° in pure water to 25.0° around TMA. These decreases in H-bond angle and length are again characteristic of a hydrophobic solute and produce a calculated positive heat capacity of hydration [31–33].

The restructuring of water around solutes is sometimes described in terms of an effective temperature [37], a lower temperature indicating more structure. In Fig. 3 the hydrogen–hydrogen radial distributions for pure water at 25°C and 5°C, and TMA hydration water at 25°C are compared. Lowering the temperature and introducing a hydrophobic solute have qualitatively similar effects —a sharpening of the radial distribution function, although the details are different. The effect of the solute occurs primarily in the first trough, while the temperature affects both first peak and first trough equally. The most widely used measure of water structure changes in simulations is the water oxygen–oxygen radial distribution function. Fig. 4 shows this radial distribution function for pure water at 25°C and 5°C, and TMA hydration water at 25°C. Lowering the temperature sharpens the distribution, as does introduction of TMA, but, in agreement with other studies [18,19], the structuring effect of a hydrophobic solute as judged by this measure is rather small. The mean H-bond length decreases to 2.93 Å at 5°C, compared to the value of 2.92 Å for water around TMA.

The effect of TMA on the H-bond angle probability distribution, $p(\theta)$, is large in contrast to the situation with the radial distribution functions (Fig. 5). In pure water at 25°C $p(\theta)$ shows a bimodal distribution, with a predominant population of nearly straight H-bonds peaking at 12°C, and a smaller population of more bent H-bonds centered at 55°C. Lowering the temperature by 20° decreases the population of more bent H-bonds slightly, resulting in a decrease in the RMS angle to 28.3°. However, introduction of TMA

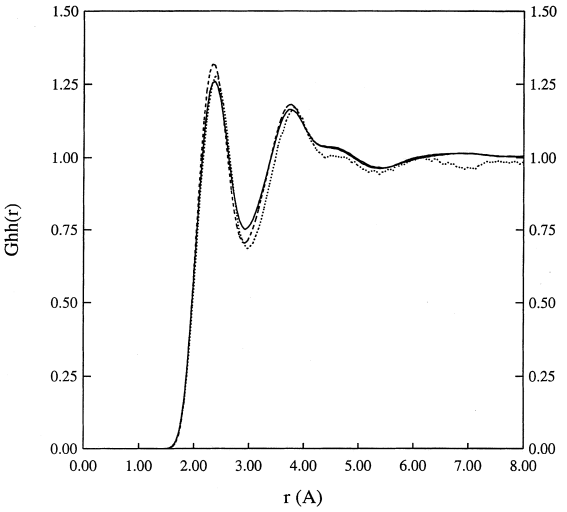

Fig. 3. The water hydrogen–hydrogen radial distribution function for pure water at 25°C (———), pure water at 5°C (- - -), and for the first shell of TMA^+ at 25°C (···). The intramolecular peak has been suppressed on this plot.

nearly eliminates the more bent H-bond population, resulting in a considerably smaller RMS angle of 25.0°.

4. Discussion

The picture that emerges from Figs. 3–5 is one in which the effect of TMA on the hydrating water structure is comparable to that induced by a 20°C temperature drop from room temperature (25°C) using radial distribution functions as a probe of water structure. In contrast, the effect on the H-bond angle is much greater than that induced by a 20°C temperature drop. Thus the H-bond angle is several times more sensitive a measure of structural changes induced by a hydrophobic solute. In addition, it is not necessary to correct $p(\theta)$ for variation in local H atom density due to solute and hydration shell exclusion, so it is simpler to obtain than solute hydration shell radial distribution functions. The correction for radial distribution functions is relatively simple for the spherical solute studied here, but becomes more difficult to evaluate accurately for more complex solute shapes.

Comparing our hydrogen–hydrogen radial dis-

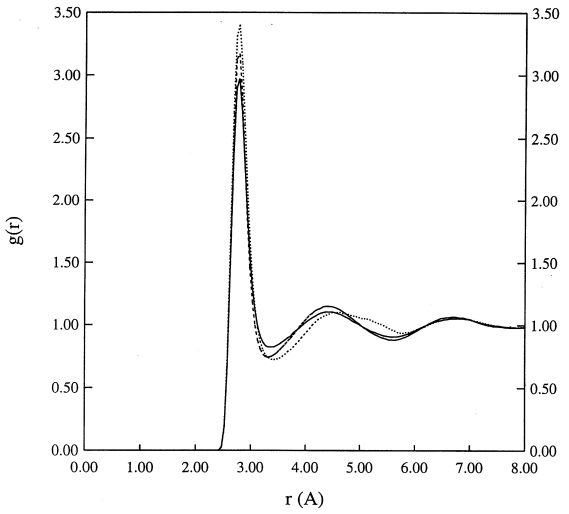

Fig. 4. Water oxygen–oxygen radial distribution function for pure water at 25°C (———), pure water at 5°C (- - -), and for the first shell of TMA^+ at 25°C (···).

tribution functions to those determined by neutron diffraction, the results for pure water are very similar (omitting the comparison of the intramolecular H-H peak), with peaks at 2.2 Å and 3.7 Å, and a trough at 2.9 Å, indistinguishable in position from those obtained from neutron diffraction [16]. This provides further evidence of realistic water structure produced by the TIP4P model. Comparing the results for water around TMA with pure water, we see significant sharpening of $g_{hh}(r)$ in the simulations, the peak to trough ratio increasing from 1.64 to 1.79, a 10% increase. The experimental results for TMA are indistinguishable from pure water [14]. However, in a later study on tetra-butyl and tetra-propyl ammonium, Turner et al. [16] saw a similar degree of sharpening to that seen in these simulations, the peak to trough ratios changing from approximately 1.58 in pure water to 1.67 for water around tetra-butyl ammonium. The 6% increase is somewhat smaller than that seen in the simulations of TMA. Our explanation of the null experimental result in the TMA solution is that at the concentration of the experiment (data for 1M TMA is shown by Turner et al. [14]) there are approximately 55 waters per solute. However, the approximate number of waters in the first shell of TMA is 30, so the structural changes could be masked by approximately 50% of the water that is outside the hydration shell. The competing effect of water structuring around the chloride anion may also further mask the hydrophobic ion structuring in the experiment. The later studies with the larger TAA ions were done at concentrations where on average all waters were in the first shell of the cation [16], so a significant ordering effect is seen, although the presence of the anion may still reduce its magnitude. Since in the simulations we directly analyze the structure of water in the first hydration shell of an isolated cation, the structural changes are not diluted by these other effects, and are larger than those seen experimentally. Another likely source of discrepancy between the simulation results and the experimental results is the fact that the simulation models for TMA as well as TIP4P water are by no means perfect. It is also noteworthy to point out that the results shown here for $g_{hh}(r)$ and for RNM parameters are for the first-shell–first-shell (1–1) interactions. However, we have found that the RNM parameters for the hydrogen bonds belonging to other classes, such as 1–2, 2–2, 2–3 etc. are not different from the RNM parameters for the hydrogen bonds in bulk water.

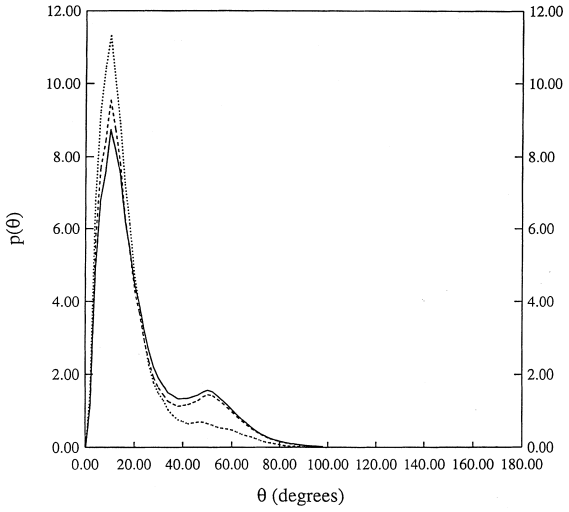

Fig. 5. The water H-bond angle probability distribution for pure water at 25°C (———), pure water at 5°C (- - -), and for the first shell of TMA^+ at 25°C (···).

5. Conclusions

Experimental data on the specific way water is structured by hydrophobic solutes is sparse, the most informative data coming from $g_{hh}(r)$ determinations using neutron scattering. Simulation of $g_{hh}(r)$ of water around the hydrophobic ion TMA^+ shows evidence for ordering similar to that seen in neutron scattering studies of the larger tetra alkyl ammonium ions TBA^+ and TPA^+, but the effects are not large. For this reason in TMA^+, the smallest of the tetra alkyl ammonium ions, we surmise that these changes might be masked experimentally by remaining bulk water or water structuring around anions, which would explain why no changes were seen for this ion in earlier neutron scattering studies. Changes in simulated $g_{oo}(r)$ indicating an increase in order are also seen, but again the effects are rather small. In contrast, much larger changes for the hydrogen bond angle distribution function $p(\theta)$ seen in the simulations indicate significant ordering; ordering, moreover, which is responsible for the positive hydration heat capacity characteristic of the hydrophobic effect. There is a high degree of orientational ordering in water, and changes in this ordering appear to play a dominant role in structure and heat capacity changes associated with solvation [33]. Since these changes can occur with relatively small changes in H–H and O–O radial distribution functions, we argue that radial distribution functions are inherently insensitive measures of the relevant structural changes. This may also account for conclusions from some previous simulations of hydrophobic solvation that there is little increase in water structure.

Acknowledgements

We thank Kelly Gallagher for helpful discussions on the radial distribution function correction. Financial support is acknowledged from the NIH (GM54105).

References

[1] H.S. Frank, M.W. Evans, J. Chem. Phys. 13 (1945) 507.
[2] K. Miller, J. Hildebrand, JACS 90 (1968) 3001.
[3] S. Cabani, P. Gianni, V. Mollica, L. Lepori, J. Soln. Chem. 10 (1981) 563–595.
[4] Y. Marcus, Biophys. Chem. 51 (1994) 111–128.
[5] A. Ben-Naim, Y. Marcus, J. Chem. Phys. 81 (1984) 2016–2027.
[6] J.T. Edsall, JACS 57 (1935) 1506–1507.
[7] G. Makhatadze, P. Privalov, J. Mol. Biol. 213 (1990) 375–384.
[8] K.P. Murphy, P.L. Privalov, S.J. Gill, Science 247 (1990) 559–561.
[9] K. Murphy, S. Gill, Therm. Acta 172 (1990) 11–20.
[10] C.H. Tanford, The Hydrophobic Effect, John Wiley and Sons, New York, 1980.
[11] W. Luck, in: F. Franks (Ed.), Water: A Comprehensive Treatise, vol. 2, Plenum, New York, 1973, pp. 235–314.
[12] M. Blandamer, M. Fox, in: F. Franks (Ed.), Water: A Comprehensive Treatise, vol. 2, Plenum Press, New York, 1973, pp. 459–492.
[13] J. Enderby, G. Neilson, in: F. Franks (Ed.), Water: A Comprehensive Treatise, vol. 6, Plenum Press, New York, 1979, pp. 1–45
[14] J. Turner, Mol. Phys. 70 (1990) 679–700.
[15] J. Turner, A. Soper, J. Finney, J. Chem. Phys. 102 (1995) 5438–5443.
[16] J. Turner, A. Soper, J. Chem. Phys. 101 (1994) 6116–6125.
[17] H.S. Frank, W.Y. Wen, Discuss. Faraday Soc. 24 (1957) 133.
[18] D. Tobias, C.L. Brooks, J. Chem. Phys. 92 (1989) 2582–2592.
[19] A. Wallqvist, Chem. Phys. Lett. 182 (1991) 237–241.
[20] C. Pangali, M. Rao, B. Berne, J. Chem. Phys. 71 (1979) 2982–2990.
[21] M. Mezei, D. Beveridge, J. Chem. Phys. 74 (1981) 622–632.
[22] P.J. Rossky, M. Karplus, J. Am. Chem. Soc. 101 (1978) 1913.
[23] C.Y. Lee, J.A. McCammon, P.J. Rossky, Chem. Phys. 80 (1984) 4448.
[24] Y.-K. Cheng, P.J. Rossky, Nature 392 (1998) 696–699.
[25] W.C. Swope, H.C. Anderson, J. Phys. Chem. 88 (1984) 6548–6556.
[26] S. Fleischmann, C. Brooks, J. Chem. Phys. 87 (1987) 3029–3037.
[27] T. Lazaridis, M. Paulaitis, J. Phys. Chem. 96 (1992) 3847–3855.
[28] T. Lazaridis, M. Paulaitis, J. Phys. Chem. 98 (1994) 635–642.
[29] S.A. Rice, M.G. Sceats, J. Phys. Chem. 85 (1981) 1108–1119.
[30] A.R. Henn, W. Kauzmann, J. Phys. Chem. 93 (1989) 3770–3783.
[31] B. Madan, K.A. Sharp, J. Phys. Chem. 100 (1996) 7713–7721.
[32] B. Madan, K.A. Sharp, J. Phys. Chem. 101 (1997) 11237–11242.

[33] K.A. Sharp, B. Madan, J. Phys. Chem. 101 (1997) 4343–4348.
[34] W.L. Jorgensen, J. Chandrasekhar, J.D. Madura, R.W. Impey, M.L. Klein, J. Chem. Phys. 79 (1983) 926.
[35] W.L. Jorgensen, J. Tirado-Rives, J. Am. Chem. Soc. 110 (1988) 1657–1666.
[36] W.L. Jorgensen, in: BOSS, Version 3.3, Copyright Yale University, New Haven, CT, 1992.
[37] R.E. Verrall, in: F. Franks (Ed.), Water: A Comprehensive Treatise, vol. 3, Plenum Press, New York, 1973.